actuators

MDPI

Article

Design, Control, and Testing of a Multifunctional Soft Robotic Gripper

A. Correia [1], T. Charters [1], A. Leite [1,2], F. Campos [1,3], N. Monge [4], A. Rocha [4] and M. J. G. C. Mendes [1,2,5,*]

1 ISEL—Instituto Superior de Engenharia de Lisboa, Instituto Politécnico de Lisboa, 1959-007 Lisbon, Portugal; a51089@alunos.isel.pt (A.C.); tiago.charters.azevedo@isel.pt (T.C.); afonso.leite@isel.pt (A.L.); francisco.campos@isel.pt (F.C.)
2 CIMOSM—Centro de Investigação em Modelação e Optimização de Sistemas Multifuncionais, ISEL—Instituto Superior de Engenharia de Lisboa, Instituto Politécnico de Lisboa, 1959-007 Lisbon, Portugal
3 UnIRE—Unit for Innovation and Research in Engineering, ISEL—Instituto Superior de Engenharia de Lisboa, Instituto Politécnico de Lisboa, 1959-007 Lisbon, Portugal
4 ESELx—Escola Superior de Educação de Lisboa, Instituto Politécnico de Lisboa, 1549-003 Lisbon, Portugal; nmonge@eselx.ipl.pt (N.M.); arocha@eselx.ipl.pt (A.R.)
5 CENTEC—Centre for Marine Technology and Ocean Engineering, Instituto Superior Técnico, Universidade de Lisboa, 1049-001 Lisbon, Portugal
* Correspondence: mario.mendes@isel.pt

Abstract: This paper proposes a multifunctional soft robotic gripper for a Dobot robot to handle sensitive products. The gripper is based on pneumatic network (PneuNet) bending actuators. In this study, two different models of PneuNet actuators have been studied, designed, simulated, experimentally tested, and validated using two different techniques (3D printing and molding) and three different materials: FilaFlex 60A (3D-printed), Elastosil M4601, and Dragonskin Fast 10 silicones (with molds). A new soft gripper design for the Dobot robot is presented, and a new design/production approach with molds is proposed to obtain the gripper's PneuNet multifunctional actuators. It also describes a new control approach that is used to control the PneuNet actuators and gripper function, using compressed air generated by a small compressor/air pump, a pressure sensor, a mini valve, etc., and executing on a low-cost controller board—Arduino UNO. This paper presents the main simulation and experimental results of this research study.

Keywords: soft robotics; multifunctional soft PneuNet actuators; soft robotic gripper; hyperelastic models; Dobot robot

Citation: Correia, A.; Charters, T.; Leite, A.; Campos, F.; Monge, N.; Rocha, A.; Mendes, M.J.G.C. Design, Control, and Testing of a Multifunctional Soft Robotic Gripper. *Actuators* **2024**, *13*, 476. https://doi.org/10.3390/act13120476

Academic Editor: Hamed Rahimi Nohooji

Received: 30 September 2024
Revised: 11 November 2024
Accepted: 18 November 2024
Published: 25 November 2024

1. Introduction

This study aimed to develop and control a soft inflatable actuator meant for a pneumatically actuated soft robotic grip for a robot arm, namely, a Dobot robot [1].

The performance of the soft robotic arm grip is dependent on the inflatable actuatorp; therefore, a set of design requirements were formulated to guide the design process: large range of motion, actuation under small amounts of pressure, and, finally, simple and fast manufacturing. Thus, the actuator must be highly compliant and manufactured with molds or additive fabrication methods [2–4].

Digital prototyping changes the paradigm of soft actuators' development. Soft actuators with a series of elastic actuators can be built with rigid materials [5] or with variable stiffness [6–8].

Although the mechanical design plays a fundamental part in soft inflatable actuators, the set of available design parameters is large: geometry, elastic material properties, actuated medium (air or water, for example), methods of fabrication (inducing specific required deformations or opposing design requirements), actuation modes, positive or negative pressure, and the list continues. Here, it is expected to rely on natural designs [9,10] for inspiration and to reduce the parameter value space.

Various geometries of linear bellow-type actuators are possible [2,4,11], and analytical models describing the stiffness of the actuators of different geometries are given [12]. Although the models presented in [13] are still designs, their geometries can be extrapolated to soft material actuators [14]. In control, a recent proposal to control a peristaltic robot inspired by inchworms can be found [15].

An extensive literature review seems to show that no all-size-fit-all design exists. This study restricts the design to an elastic inflatable actuator under positive pressure, namely, PneuNet soft actuators [7]. PneuNet (pneumatic networks) consists of a series of channels and chambers inside an elastomer. These channels inflate when pressurized, expanding in the most compliant regions and, therefore, motion. The behavior of PneuNet actuators can be customized by modifying the geometry of their chambers and the materials' properties. PneuNet for soft robotic actuators combines high actuation rates with high actuator reliability [2,7,12].

PneuNet actuators are characterized by their inherent softness and compliance, making them ideal for scenarios where rigid actuators are unsuitable. They are also lightweight, which benefits systems where weight is a critical factor. These two advantages were significant in deciding which approach to take for the Dobot gripper. Additionally, their softness ensures safer interactions, particularly in human–robot interfaces or for gripping touch-sensitive materials. However, designing PneuNet actuators to achieve specific behaviors requires meticulous planning, design and optimization, and time. The performance of a PneuNet actuator is also influenced by changes in pressure, tending to have slower response times compared to other types of actuators. Considering some of these advantages and disadvantages, this paper presents the development of PneuNet-type actuators for a Dobot robot gripper.

This paper is divided into the following sections: Section 2 presents the materials and methods used in this study; Section 3 presents the simulation and experimental results obtained and their discussion; and Section 4 presents the conclusions.

2. Materials and Methods

2.1. Modeling Bending Behavior of PneuNet Actuators

Modeling PneuNet actuators analytically remains complex due to their construction using entirely flexible, hyperelastic materials. Their inherent bending curvature and stiffness change with varying input pressure [16]. This section aims to summarize the mathematical modeling that establishes the relationship between the curvature/bending angle of the actuator and the input pressure. Later in this work, the simulation and experimental results for these two variables are presented for the actuators developed.

Majidi et al. [17] established a mathematical correlation between the input pressure and the bending curvature of a PneuNet actuator with a fixed chamber height (Figure 1 and Equation (1)). This model, based on the principle of minimum potential energy, shows that the actuator's curvature kp is directly proportional to the input pressure (P) as follows:

$$k_P = \frac{6H^2c}{Et^3x}P = DP \quad where\ D = \frac{6H^2c}{Et^3x} is\ constant \tag{1}$$

The chamber geometry and the material's properties influence the constant (D). It is assumed that the modulus of elasticity (E) remains constant, simplifying the model for hyperelastic materials, and the impact of gravity is disregarded. Another significant contribution in this area is the bending angle model introduced by Alici et al. in their study [18]. They formulated a method to predict the bending angle of a PneuNet actuator with a fixed chamber height based on input pressure, considering the actuator as a cantilever beam (Equation (2)).

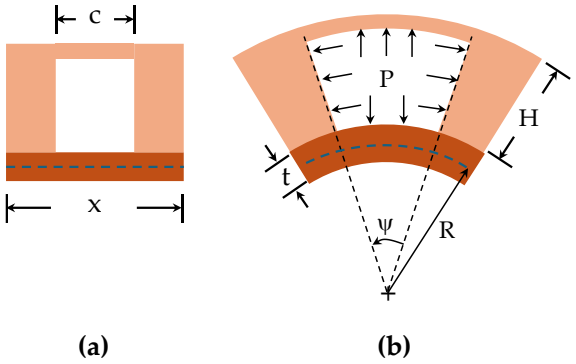

Figure 1. PneuNet chamber (**a**) before and (**b**) after inflation (adapted from [17]).

By applying the Euler–Bernoulli beam theory and assuming that the actuator bends into a uniform curvature, they derived the following steady-state relationship:

$$\theta(P) = \underbrace{\frac{L_i A^2 e}{A_w E^2 I}}_{C} P^2 + \underbrace{\frac{L_i A e}{EI}}_{D} P = CP^2 + DP \quad (2)$$

Constants (C) and (D) are influenced by the geometry of the chambers and the material properties, where A and A_w are the cross-sectional areas of the chamber, I is the area moment of inertia, and e is the offset between the center of pressure and the neutral axis of the chamber. This model considers the chamber and gap between two chambers as a single unit with a length of L_i. In this context, the bending angle changes nonlinearly with input pressure, making it a potentially better model for PneuNet constructed with hyperelastic materials, as constant (C) is inversely related to the square of (E). Assuming a constant curvature, if a PneuNet actuator is anchored at one end and is free to bend at the other, the bending moment (M) generated by the pressure force and the internal area of the pneumatic chambers will move the actuator from its initial to its final position [16].

2.2. Modeling of the Actuators and Gripper

Two different models of PneuNet actuators have been 3D-modeled in Solidworks Student® and fabricated with fast prototyping methods: type 1 (Figure 2a), inspired by Yap et al. [19], and type 2 (Figure 2b), inspired by Patel et al. [20]. Although type 1 and 2 actuators, shown in Figure 2, were inspired by the geometry of the actuators in the references in question, both had to be modified taking into account the scale factor and the needs of a soft gripper project for a Dobot robot, whose soft gripper dimensions immediately require adjustments to the dimensions of the actuator chambers (reducing the length and thickness of the walls) and an assertive reduction in the number of chambers for each actuator model. In addition, since this is a soft gripper design, some roughness was added to the actuator tip for better grip. The models were also modified so that they could be easily used and inserted into the new gripper coupling base designed for the Dobot robot. The type 1 model is also produced with two-half molds, optimized for building actuators in one piece, without the need for two-stroke production, reducing the associated production errors, and with an internal spine approach that is removed at the end through the same hole where the compressed air tube will be inserted.

Two different production methods were used, i.e., (1) 3D printing by fused deposition modeling (FDM), where Filaflex 60A filament was used, and (2) fabricated molds, where two distinct silicones were used: DragonSkin Fast 10 and Elastosil M4601 A/B. FilaFlex 60A was used because, among the several types of this filament, it had lower Shore hardness and higher elongation.

In Figure 3, PneuNet actuators of type 1, fabricated with FDM-printed molds, using the two silicones are seen: Figure 3a DragonSkin Fast 10 and Figure 3b Elastosil M4601 A/B.

The two models in Figure 2 were used in this study, but model type 1 (in Figure 2a) was the one chosen for mold production as it worked very well for the soft gripper intended for the Dobot robot. Type 2 models (in Figure 2b) were not produced using this technique.

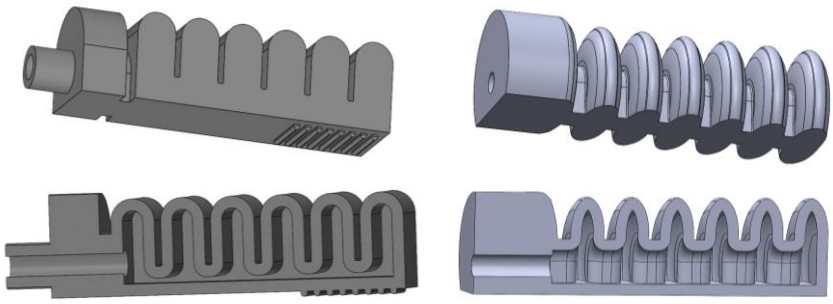

(**a**) (**b**)

Figure 2. PneuNet actuators modeled: (**a**) type 1, inspired by [19] and made with Elastosil and DragonSkin Fast 10 (using molds) and with Filaflex 60A filament by FDM; (**b**) type 2, inspired by [20], made with Filaflex 60A filament by FDM.

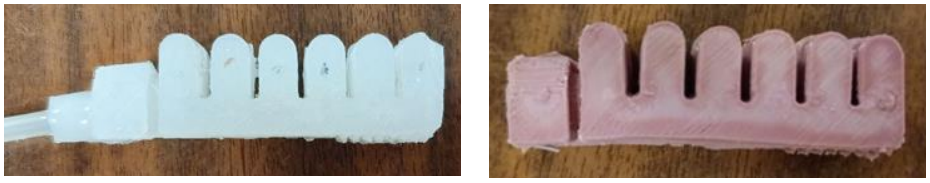

(**a**) (**b**)

Figure 3. PneuNet actuators of type 1 fabricated with molds (**a**) made with DragonSkin Fast 10 silicone and (**b**) made with Elastosil M4601 A/B silicone.

Table 1 shows the properties of the two silicones and Filaflex 60A filament used in this study.

Table 1. Material properties.

	DragonSkin Fast10 [21]		**Elastosil M4601 A/B [22]**		**Filaflex 60A [23]**	**Unit**
Component	A	B	A	B	-	
Mixing ratio in weight	50	50	90	10	-	%
Density at 23 °C	1.07		1.14	1.01	1.07	g/cm^3
Cure time	1.15		12		-	h
Viscosity a 23 °C	23,000		10,000		-	MPa.s
Hardness	10		28		63	Shore A
Young Modulus	0.13 [24]		0.4835 [12]		2.5	Mpa
Tensile strength	3.3		6.5		26	Mpa
Poisson's Ratio	0.48–0.50		0.499 [12]		0.49–0.50	
Tear strength	-		>30		40	N/mm
Elongation at tear	1000		700		950	%

Both mold halves are in Figure 4a,b. To obtain the interior cavity of the PneuNet actuator, a third component, acting as a core mold part, had to be assembled beforehand (see Figure 4c, depicting both mold halves and the central core). The uncured silicone was put in both halves of the mold, one containing the rigid core, held in place due to its L

shape at one end. The two mold halves were closed, centered by the six centering pins (Figure 4), smashing the silicone against the core and mold walls up to the complete closing of the mold. The excess air and liquid silicone material could be extracted from the mold holes and parting line.

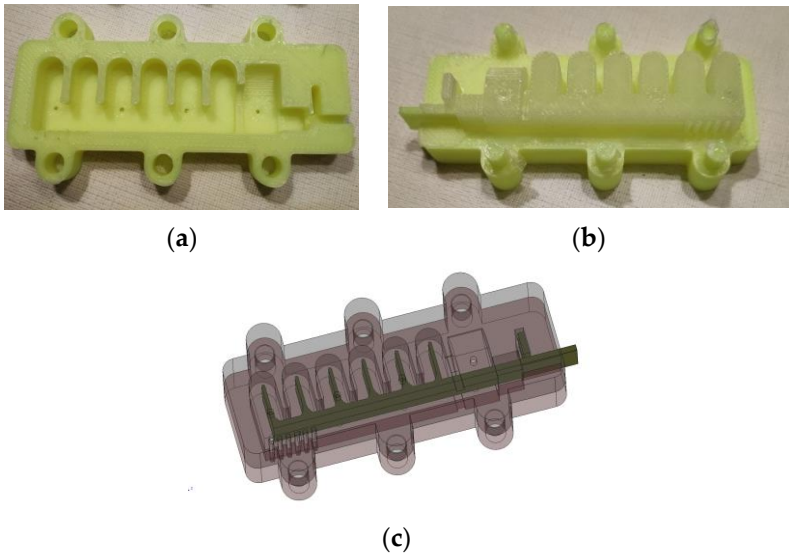

(**a**) (**b**)

(**c**)

Figure 4. FDM-printed mold for PneuNet actuators of type 1: (**a**) half of the mold; (**b**) top half of the mold along with the PneuNet actuator molded with DragonSkin Fast 10 and inner core; and (**c**) 3D model of the mold and inner core.

After the silicone curing, the plastic core can be extracted from the PneuNet actuator by pulling it with pointed pliers or other tools from the orifice where the air enters the actuator. The molds and inner core were made from Polylactic Acid (PLA). Different solutions were tested, e.g., having a core made of Polyvinyl Alcohol (PVA) to be dissolved with water, but this proved unsuccessful due to the water reacting with silicone.

The types 1 and 2 PneuNet actuators were also fabricated with FDM 3D printing with Filaflex 60A filament (Figure 5). The type 2 models were used only with 3D printing and FilaFlex 60A filament (Figure 5b) and compared with the type 1 model also in Filaflex 60A. In this printed material, the type 1 model is too rigid for a soft gripper (compared to the silicone model) working at much higher pressures, so we looked for another model (type 2) which mechanically proved to work better and be much more flexible when printed in Filaflex 60A filament, also working at much lower pressures (as we will see in the results obtained) to make it possible to grip sensitive objects.

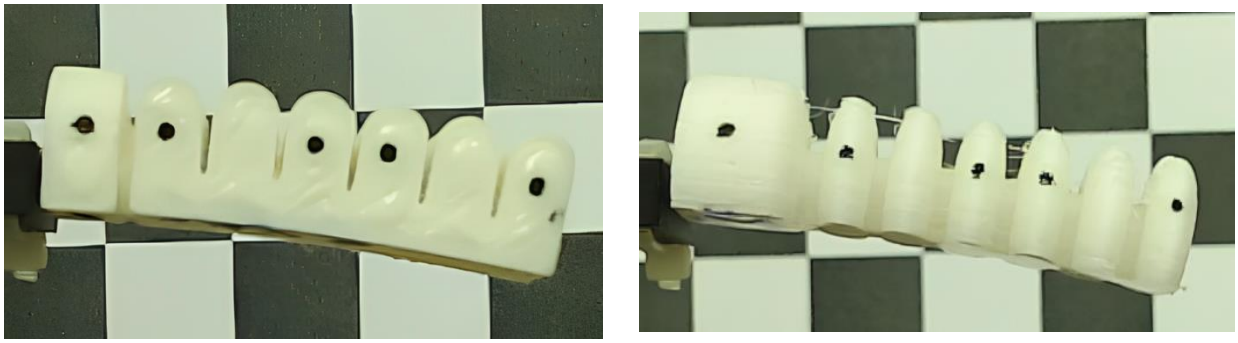

(**a**) (**b**)

Figure 5. PneuNet actuators fabricated: (**a**) type 1, inspired by [19], and (**b**) type 2, inspired by [20]. Both actuators were 3D-printed with FilaFlex 60A filament by FDM.

In Figure 6, the PneuNet actuators, obtained by FDM (Figure 6a) and molds (Figure 6b), can be seen mounted in the Dobot gripper (it uses three actuators). The three actuators fit into the coupling base (Figure 6c) of the gripper which was FDM-printed with the PLA material.

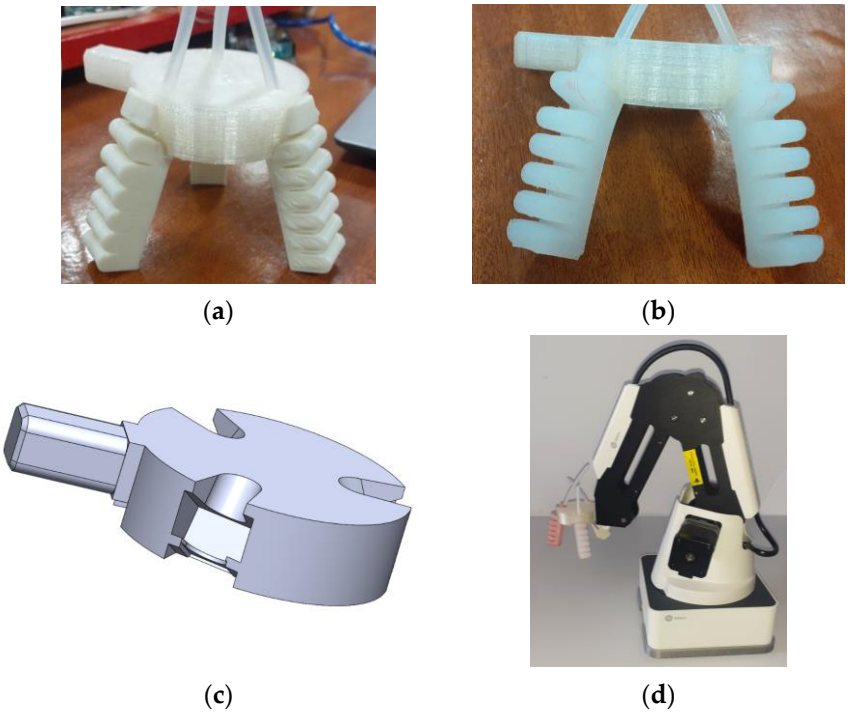

Figure 6. PneuNet actuators of type 1 mounted on the PLA FDM-printed coupling base. (**a**) fabricated with FDM using Filaflex 60A filament and (**b**) made with DragonSkin Fast 10 silicone by molding, (**c**) gripper coupling base, and (**d**) Dobot robot with soft gripper installed.

2.3. Control of the Soft Gripper

To demonstrate a use case application of the proposed soft actuators, a robotic gripper with three soft actuators was integrated into the pick and place operations of a Dobot robot (Figure 6d). This section describes the control system used to drive the gripper's grab/release cycles in the context of these tasks.

2.3.1. Pneumatic and Electronic Circuits

The pneumatic circuit that was devised to supply pressurized air into the soft actuators consists of (1) a mini diaphragm air pump [25], (2) a 2-way, 2 position solenoid valve [26], (3) a throttle valve [27], and (4) a pressure sensor [28], connected as depicted in Figure 7.

The control logic is run on an Arduino Uno board, which receives the analog reading from the pressure sensor and outputs two control signals that regulate the current through the solenoid valve and the pump via two power transistors, as shown in Figure 8. The goal of the control system is to drive simple grab/release cycles of the gripper; thus, the pressure in the actuators should follow a waveform that goes from atmospheric pressure (release) to a reference pressure (grab) and back to atmospheric pressure (release). Here, pressure is the single controlled variable, and a desired curvature (kp) of the actuators is achieved by selecting the corresponding pressure, as given by the pressure–curvature relation described in Section 2.1. An alternative to this approach would be to embed strain sensors into the soft actuator [29,30] and implement a control loop that directly targets curvature.

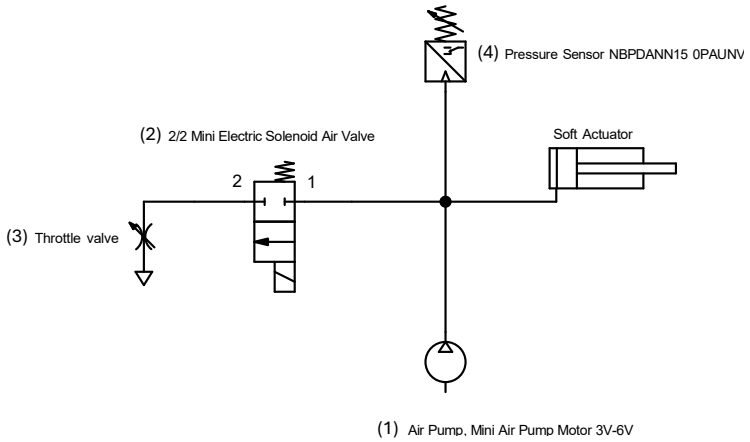

Figure 7. Pneumatic circuit that regulates air flow in/out of the soft gripper.

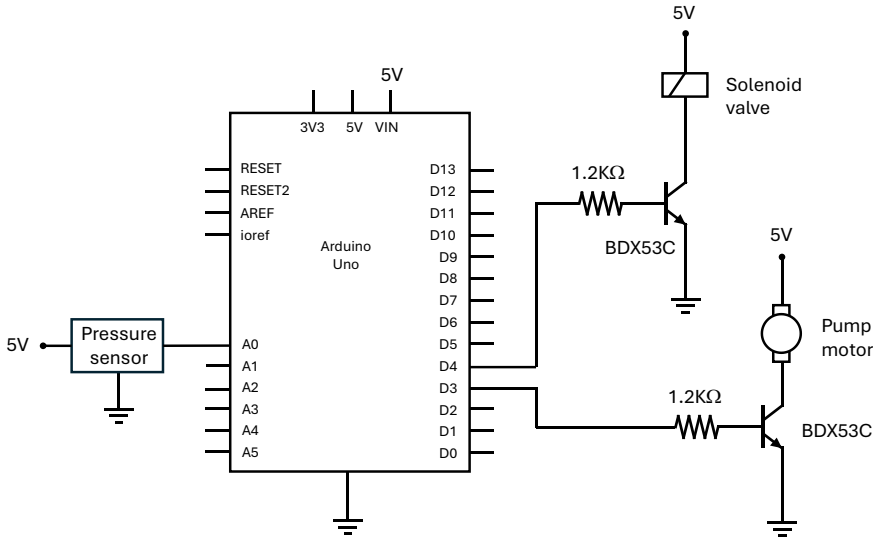

Figure 8. Electronic circuit of the control system that drives gripper actions.

In the present study, pressure is mainly controlled by modulating the speed of the pump. This is in strong contrast to the most common approach, which involves using a constant source of pressurized air combined with two on/off solenoid valves that regulate the airflow in and out of the actuator [31–34]. In this approach, pressure is controlled by switching the valves at a high frequency, thereby regulating the airflow into and out of the actuator. To achieve this, the valves are driven by PWM signals, in which duty cycles take the role of the control action, i.e., they are continuously adjusted to achieve the desired pressure. In contrast, in the current proposed approach, the valve is commanded by a digital signal that occasionally changes state, whereas a PWM signal drives the pump.

It follows that a pressure increase is achieved by closing the valve and powering the pump through a suitable control law while pressure reduction is attained by turning off the pump and opening the valve. Now, while the PWM signal can continuously modulate the pressure rise, pressure reduces abruptly when the valve is opened. To avoid a sudden fall in pressure due to the on/off nature of the valve, a throttle valve is connected to the valve exit. In this way, the pressure falls more slowly, resulting in a slightly slower opening of the gripper, which, on the other hand, reduces oscillations. But most important is the effect of the throttle valve when the transient response of the system is oscillatory. In this case, a fast decrease in pressure, associated with the inherent delays of the pneumatic system, gives rise to oscillations. This can be attenuated with the introduction of a throttle valve, which contributes to an amount of damping that can be adjusted to mitigate that behavior.

The addition of damping through a pneumatic component was used previously in [33,34], where the authors resorted to a tube fitted with a porous plug that acts as a pneumatic low pass filter.

Past research on soft actuator control has led to sliding mode controllers [34–36], model reference adaptive controllers [37], and robust adaptive controllers [30,31], among others. The controllers envisaged here have the task of opening and closing the gripper as desired. However, if the soft actuators are to be used in a legged robot, for example, oscillator controllers such as motor neuron controllers [38] would be more suitable. The use of advanced controllers such as these is justified by the inherent challenges in soft actuator systems, in particular, the nonlinearities due to the hyperelasticity of the material and the PneuNet geometry, the nonlinear behavior of pneumatic components, and the delays in air distribution [31]. Still, situations exist where simpler controllers, such as PIDs, can be used, with the benefit of a more straightforward implementation and ease of reconfiguration, possibly at the cost of lower performance. In this regard, when selecting a controller for soft actuators, it should be remembered that an intrinsic advantage of these actuators is their compliance, increasing tolerance to errors. Given the simplicity of the task of opening/closing the soft gripper, and the acceptable tolerance to actuator position errors, two simple strategies, proportional/integral (PI) and on/off, are considered in this study. The resulting control systems are nonlinear since, as mentioned before, different rules concerning the pump and valve are defined for positive (pressure rise) and negative (pressure reduction) control actions. Also, the valve behavior is nonlinear by nature. In the first control strategy, henceforth denoted as nonlinear PI, the pump's duty cycle is determined from the pressure error and accumulation of error. The second is an on/off controller, where both the valve and the pump have binary states.

2.3.2. Nonlinear PI Control

The PI control action is computed by combining a term proportional to the error and a second term proportional to the integral of the error [39]. This is used to calculate the duty cycle of the pump. However, when the control action is negative, the pump must be stopped, and the valve actuated instead. This mechanism can be implemented through Algorithm 1.

Algorithm 1 Nonlinear PI Controller

```
integral = 0
repeat:
    error = reference–pressure
    integral = integral + error × dt
    u_PI = K_p × error + K_i × integral
    if u_PI ≥ 0 then
        u_pump = u_PI
        u_valve = closed
    else
        u_valve = open
        u_pump = 0
```

In the above algorithm, the symbols used are as follows:
Reference—desired pressure [bar];
Pressure—actual pressure [bar];
Dt—sample time [s];
U_{PI}—proportional/integral control action [%];
K_p—proportional gain [bar^{-1}];
K_i—integral gain [bar^{-1} s^{-1}];
U_{pump}—duty cycle of the pump [%];
U_{valve}—valve state [on/off].

2.3.3. On/Off Controller

In a typical on-off controller, there is an actuator with two possible states, on and off [39], and state changes occur when the control error exceeds a specific interval set around zero. This typically leads to oscillating behavior with switching times that depend on the gap between the interval limits.

In this case, there are two actuators, the pump and the valve, and an on/off rule can be set for each, which offers more flexibility in designing the controller behavior. Essentially, the pump should be switched on when the error is positive and exceeds the positive threshold. The valve should be opened when the error is negative and falls below the negative threshold. In addition, each actuator should be switched off when the error crosses zero. Accordingly, the proposed on/off controller can be described by Algorithm 2:

Algorithm 2 On/Off Controller

```
u_pump = 0
u_valve = closed
repeat:
    if e > threshold then
        u_pump = PWM_ON
    if u_pump > 0 and e < 0 then
        u_pump = 0
    if e < −threshold then
        u_valve = open
    if u_valve = open and e > 0 then
        u_valve = closed
```

Where PWMOn is a constant duty cycle selected for the on state of the pump, and threshold is the maximum allowed error above which a control action is triggered.

3. Simulation and Experimental Results

3.1. Introduction to Simulation Results

This section explains the numerical simulation of the PneuNet actuators, fabricated with three different materials (two silicones with molds and Filaflex 60A by FDM). The numerical simulation was performed using the Finite Element Method (FEM) with the student version of software ANSYS Workbench® 2024 R1 Student version.

The FEM was used to simulate the physical behavior of the PneuNet models, having different geometries and materials, subjected to several input pressures, in this way helping to choose the best material, thicknesses, etc. for the application. It was very important to have a virtual verification tool of the complete bending behavior of PneuNet actuators, before producing the final printing or molds, and also to compare the deformation between the fabricated and FEM models afterwards.

Since elastomeric rubbers do not have linear elastic behavior over deformation and have an enormous elastic extension, they should be modeled with hyperelastic material model in the FEM software, by performing, in this case, a nonlinear bending simulation. The hyperelastic material models used were the second-order Mooney–Rivlin and the third-order Yeoh.

The Finite Element used was a 10-node quadratic tetrahedral solid element. The applied boundary conditions were fixed support at the proximal end of the actuators in contact with the adapter and constant static pressure applied normal to all inner walls of the actuators. Contact interactions between the outer walls of each chamber are included by enabling a self-contact, frictionless surface-to-surface method in the FEM software. Gravity acceleration was also included in the analysis. Only static studies were made with one pressure load step, implemented in a ramped form in several small time substeps, due to nonlinearity of the model. Capture curvature and proximity were applied with the standard options of Ansys. Proximity size function sources were applied to faces and edges.

Geometry meshing was optimized based on the size limitations of the FEM software and the computational efficiency and accuracy of the deformation, and a higher mesh density was used in regions with stress concentrations and smaller volumes and coarser mesh in less critical regions. The resultant maximum element size was around 1.5 to 2 mm, being smaller near the smaller regions at the chamber's connection zone. The number of elements is indicated in each model section results and is between 21,000 and 24,000.

As Yap et al. [19] noted, the 3D-printed elastomer can have an anisotropic behavior. They performed tensile tests with polymers printed in three different directions, namely, longitudinal, transverse, and crosswise. They conclude that, at the same strain level, the test pieces printed in the longitudinal orientation experienced the highest stress. They also observed that the trends in the stress–strain curves were similar in all orientations.

Since the highest and most representative strains of PneuNet actuators occurred in the longitudinal direction, they only considered constitutive model fitting for the material printed with this direction. In the present study, the same assumptions are made, i.e., the several models' hyperelastic properties are obtained from the literature for the material printed in the longitudinal direction.

Using the highest elastic modulus and rupture level stress–strain curves (in the longitudinal direction), the FEM model is somehow more rigid and attains lower strains for the same level of stress, but it should be a closer approximation to reality in terms of the printing direction.

3.2. Hyperelastic Material Models

Both silicones were studied successfully by other authors using the third-order Yeoh hyperelastic model: Ref. [40] studied DragonSkin Fast 10, and [7] studied Elastosil M4601 A/B.

The third-order (N = 3) Yeoh model strain energy potential is given by Equation (3) [41]:

$$W = \sum_{i=1}^{N} C_{i0}\left(\bar{I}_1 - 3\right)^i + \sum_{k=1}^{N} \frac{1}{d_k}(J-1)^{2k}, \quad (3)$$

where $\bar{I}_1$ is the first deviatoric strain invariant;

J is the determinant of the elastic deformation gradient;

N, C_{i0}, and d_k are material constants.

For the FDM 3D-printed material, FilaFlex 60A, the second-order Mooney–Rivlin model was applied, as also performed by [42]. In Filaflex 60A, the Mooney–Rivlin (second-order) model was used because of the availability of papers about this new material Filaflex 60A. On the other hand, with Dragon Skin Fast 10 and Elastosil M4601 A/B, because of their hyper elasticity, the most accurate model for use is the Yeoh (third-order) as its proven in papers.

The second-order (N = 2) Mooney–Rivlin model strain energy potential is given by Equation (4) [41]:

$$W = C_{10}\left(\bar{I}_1 - 3\right) + C_{01}\left(\bar{I}_2 - 3\right) + \frac{1}{d}(J-1)^2, \quad (4)$$

where $\bar{I}_1$ and $\bar{I}_2$ are the first and second deviatoric strain invariants, respectively. C_{10} and C_{01} are material constants, characterizing the deviatoric deformation of the material. d is the material incompressibility parameter. Table 2 presents the hyperelastic material properties used in the models.

Table 2. Hyperelastic material model properties used: Yeoh and Mooney–Rivlin.

Hyperelastic Model	Parameter	Material	Material	Units
		Dragon Skin Fast 10 [40]	Elastosil M4601 A/B [7]	
Yeoh (third-order)	C_{10}	0.036	0.11	Mpa

Table 2. *Cont.*

Hyperelastic Model	Parameter	Material	Material	Units
	C_{20}	2.50×10^{-4}	0.02	Mpa
	C_{30}	2.3×10^{-5}	0	Mpa
	D_1, D_2, D_3	0	0	$(Mpa)^{-1}$
		Filaflex 60A [42]		
Mooney–Rivlin (second-order)	C_{10}	0.87897		Mpa
	C_{01}	1.634		Mpa
	d	0		$(Mpa)^{-1}$

3.3. FEM and Experimental Results' Comparison

In this section, FEM and experimental results are shown and analyzed. FEM total deformation results of the two actuator types and three materials are shown for several input pressures. Then, measured angles, both in FEM and experimental, for one extreme situation are compared.

3.3.1. Type 1 Silicone Actuators' Results

The PneuNet actuator of type 1 is shown in Figure 9 in a deformed shape. The model mesh was generated with 21,591 elements and 36,565 nodes. In this figure, only the effect of gravity is observed, as no internal pressure input was applied to the model at this stage.

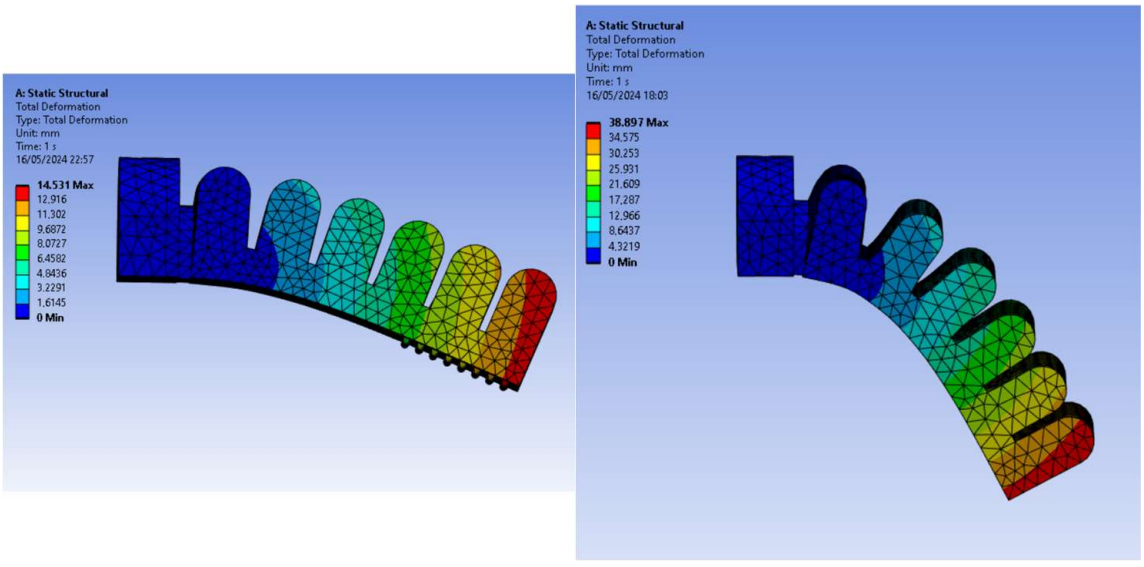

(**a**) (**b**)

Figure 9. PneuNet actuators of type 1 FEM deformation results obtained for (**a**) Elastosil M4601 A/B silicone and (**b**) DragonSkin Fast 10 silicone for 0 kPa input pressure.

As explained, simulations were carried out on both silicones' actuator types using the Yeoh hyperelastic model. Given the contrasting properties of the two silicones, different pressure ranges were simulated for each. Specifically, for the DragonSkin Fast 10, a pressure range from 0 kPa to 40 kPa (0.4 bar) was used, and for Elastosil M4601 A/B, a pressure ranged from 0 kPa to 100 kPa (1 bar) was used.

In Figure 10, both FEM models can be seen for the pressure of 40 kPa (0.4 bar).

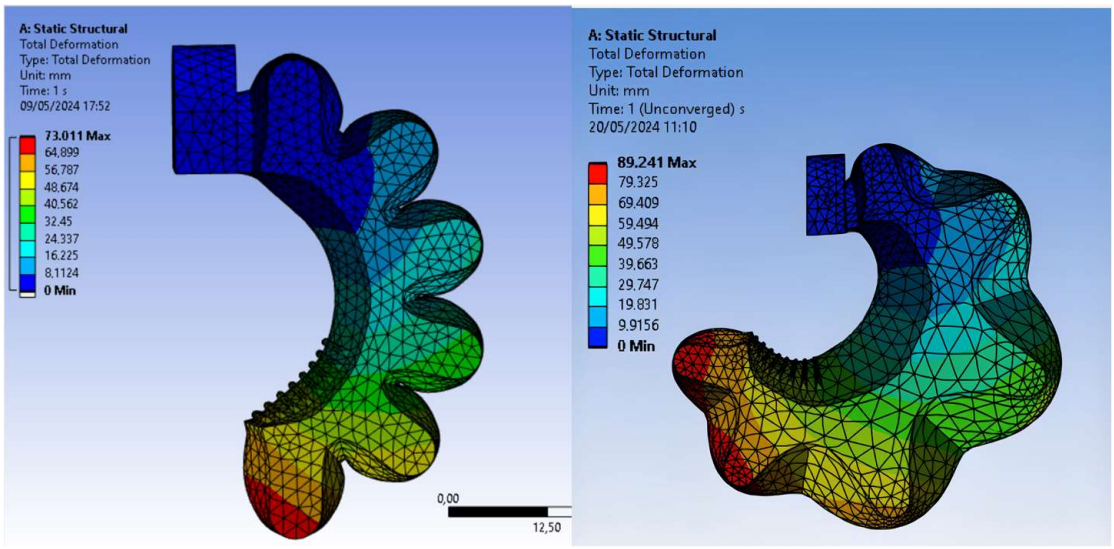

(**a**) (**b**)

Figure 10. PneuNet actuators of type 1 FEM deformation results were obtained for (**a**) Elastosil M4601 A/B silicone and (**b**) DragonSkin Fast 10 silicone for 40 kPa (0.4 bar) input pressure.

In Figure 11, a comparison is made for Elastosil M4601 A/B silicone between the FEM model (Figure 11a) and the real actuator (Figure 11b), both subjected to the maximum pressure of 100 kPa (1 bar). The experimental model rotation angle was measured with the Kinovea 2023.1 software and has the value of 115.1°. The FEM model angle was 114.8°, which gives a very good approximation.

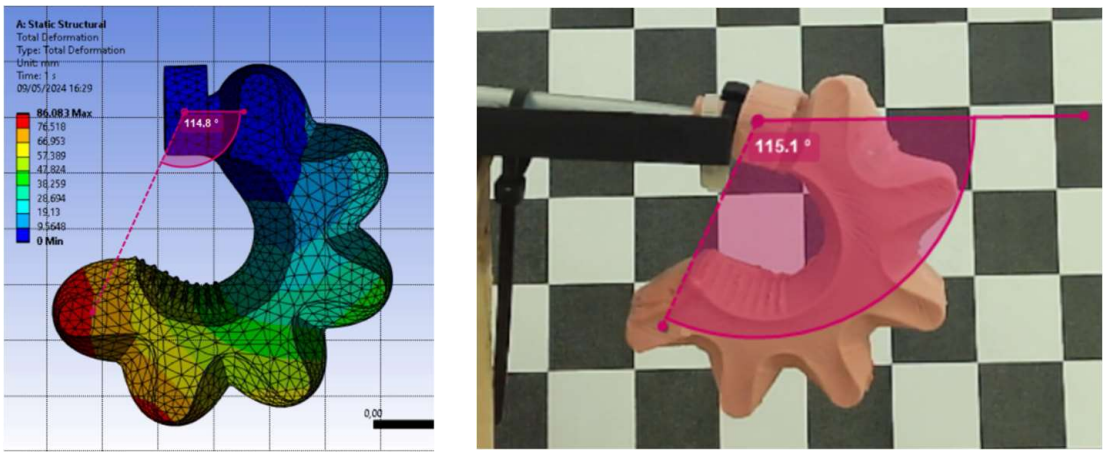

(**a**) (**b**)

Figure 11. PneuNet actuator of type 1 made of Elastosil M4601 A/B silicone comparison for 100 kPa (1 bar) input pressure: (**a**) FEM model with measured angle and (**b**) real actuator screenshot, made with the Kinovea software, with a measured angle.

In Figure 12, the same type of comparison as Figure 11 is made, but in this case for the Dragon Skin Fast 10 material with the maximum pressure of 40 kPa (0.4 bar). The experimental model measured rotation angle has the value of 124.9°. The obtained angle for the FEM model was 125.9°, having 1 degree of difference, which gives an excellent approximation.

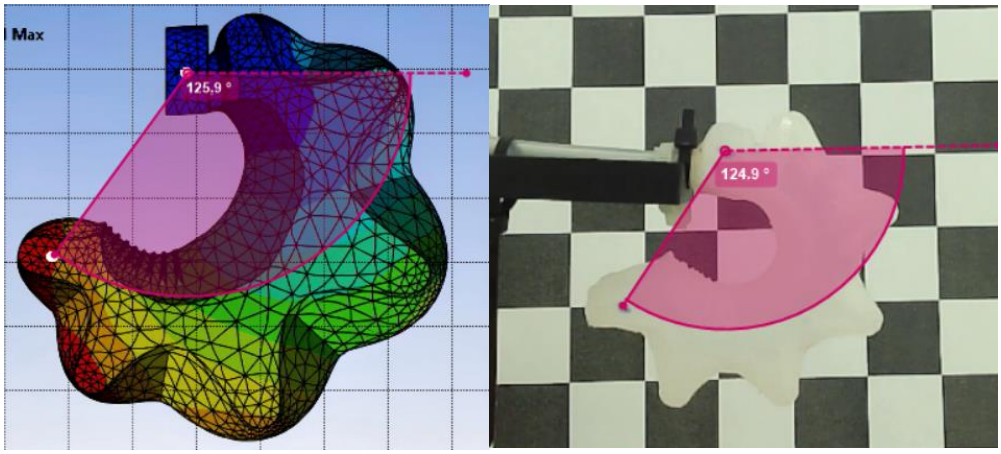

(**a**) (**b**)

Figure 12. PneuNet actuator of type 1, made of DragonSkin Fast 10 silicone, comparison for 40 kPa (0.4 bar) input pressure: (**a**) FEM model with measured angle and (**b**) real actuator screenshot, made with the Kinovea software, with a measured angle.

Figures 13 and 14 show the angular behavior curves (bending angle vs. pressure) obtained experimentally and by FEM simulation of the type 1 actuators and with the two types of silicones used. The simulation and experimental bending angle consistently follow the nonlinear models used in the simulation and prove the nonlinear bending angle model of Equation (2). The experimentally built actuators had a more linear behavior, probably due to construction details and real material behavior. To bring the two curves closer together, the parameters of the models should be adjusted to the reality obtained experimentally.

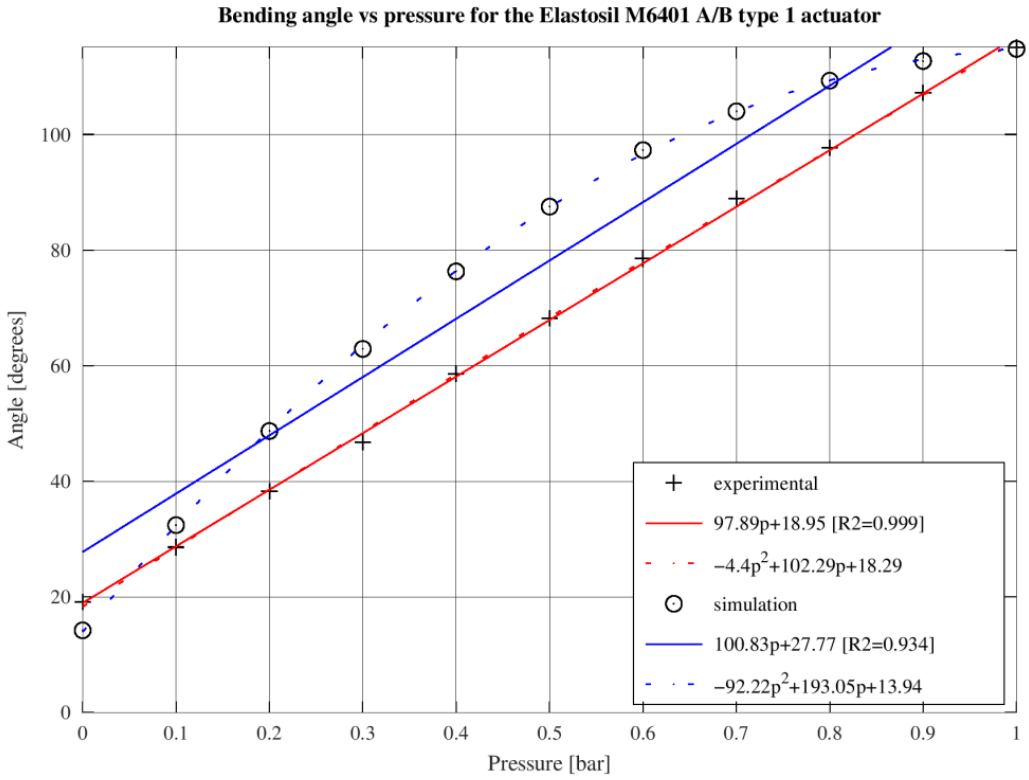

Figure 13. Bending angle vs. pressure for the Elastosil M6401 A/B type 1 actuator. Experimental data and simulation results.

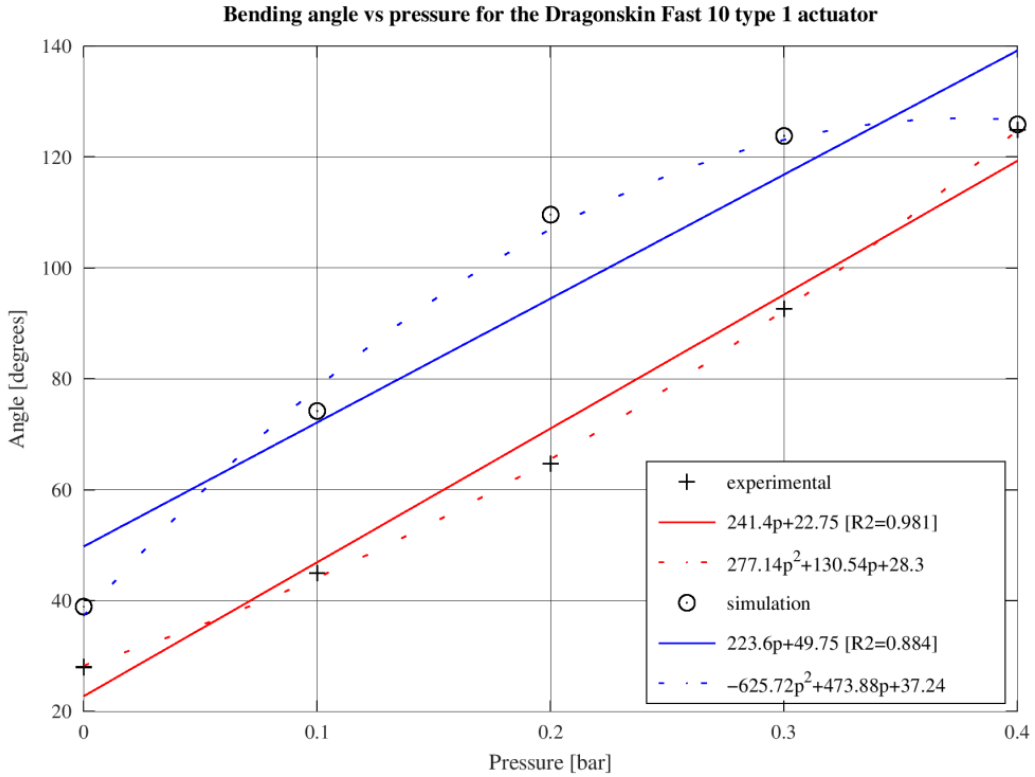

Figure 14. Bending angle vs. pressure for the Dragonskin Fast 10 type 1 actuator. Experimental data and simulation results.

3.3.2. Type 1 and 2 Actuator Results with FDM Filaflex 60A

This subsection addresses the simulation and experimental results of the actuators made with FDM Filaflex 60A.

Figure 15a shows the type 1 model in a deformed shape due to gravity and no pressure being applied. The model mesh was generated with 21,591 elements and 36,565 nodes. Figure 15b shows the type 2 model, which has 23,702 elements and 39,896 nodes, under the same conditions.

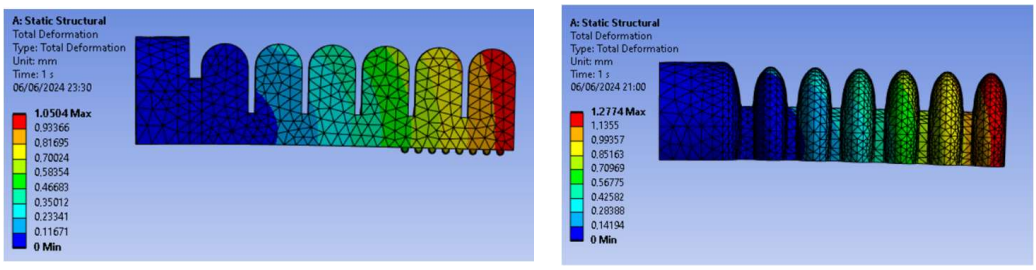

(**a**) (**b**)

Figure 15. FEM deformation results of PneuNet actuators obtained for (**a**) type 1 and (**b**) type 2, both for Filaflex 60A material obtained by FDM, and no input pressure.

In Figure 16, both FEM models can be seen for the pressure of 180 kPa (1.8 bar). The type 2 actuator produces a larger bending angle for the same pressure.

In Figure 17, a comparison is made for the type 1 actuator, between the FEM model (Figure 17a) and the real actuator (Figure 17b), both subjected to the maximum pressure of 250 kPa (2.5 bar). The experimental model rotation angle was measured with the Kinovea software and has a value of 57.5°. The FEM model angle was 29.2°, which gives a very bad

approximation of the experimental value. The FEM model properties, among others, must be investigated.

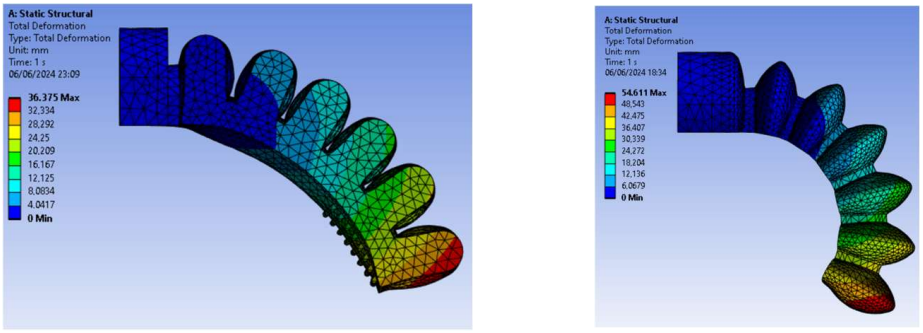

(**a**) (**b**)

Figure 16. FEM deformation results of PneuNet actuators obtained for (**a**) type 1 and (**b**) type 2, both for Filaflex 60A material obtained by FDM, and 180 kPa (1.8 bar) input pressure.

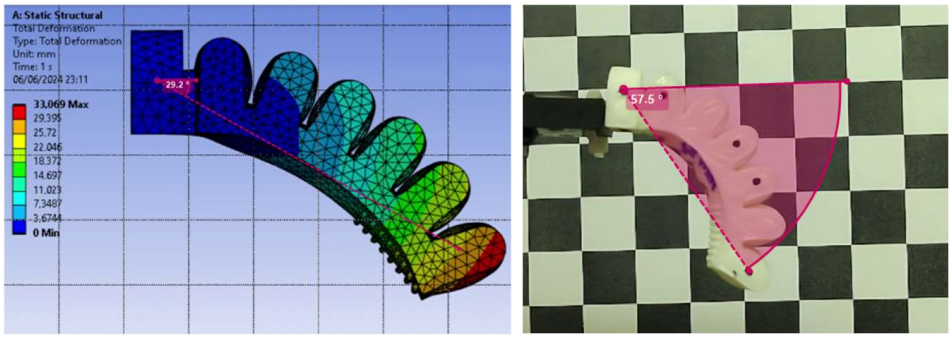

(**a**) (**b**)

Figure 17. PneuNet actuator of type 1, made of Filaflex 60A FDM filament, comparison for 250 kPa (2.5 bar) input pressure: (**a**) FEM model with measured angle and (**b**) real actuator screenshot, made with the Kinovea software, with a measured angle.

In Figure 18, the same comparison is made for type 2 actuator. The experimental model rotation angle was measured as 59°. The FEM model angle was 43.3°, which gives a better approximation of the experimental result than the one obtained for type 1, with Filaflex 60A.

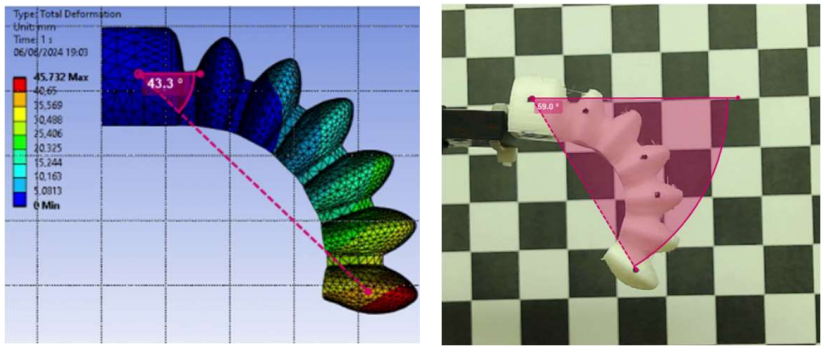

(**a**) (**b**)

Figure 18. PneuNet actuator of type 2, made of Filaflex 60A FDM filament, comparison for 180 kPa (1.8 bar) input pressure: (**a**) FEM model with a measured angle and (**b**) real actuator screenshot, made with the Kinovea software, with a measured angle.

Figures 19 and 20 show the angular behavior curves (bending angle vs. pressure), obtained experimentally and by FEM simulation of the type 1 and 2 actuators and with the Filaflex 60A filament. The simulation and experimental bending angle also consistently follow the nonlinear models used in simulation and support the nonlinear bending angle model of Equation (2). The 3D-printed actuators had a more linear behavior, probably due to 3D printing construction details and intrinsic material behavior. To bring the two curves closer together, the parameters of the models should be adjusted to the reality obtained experimentally.

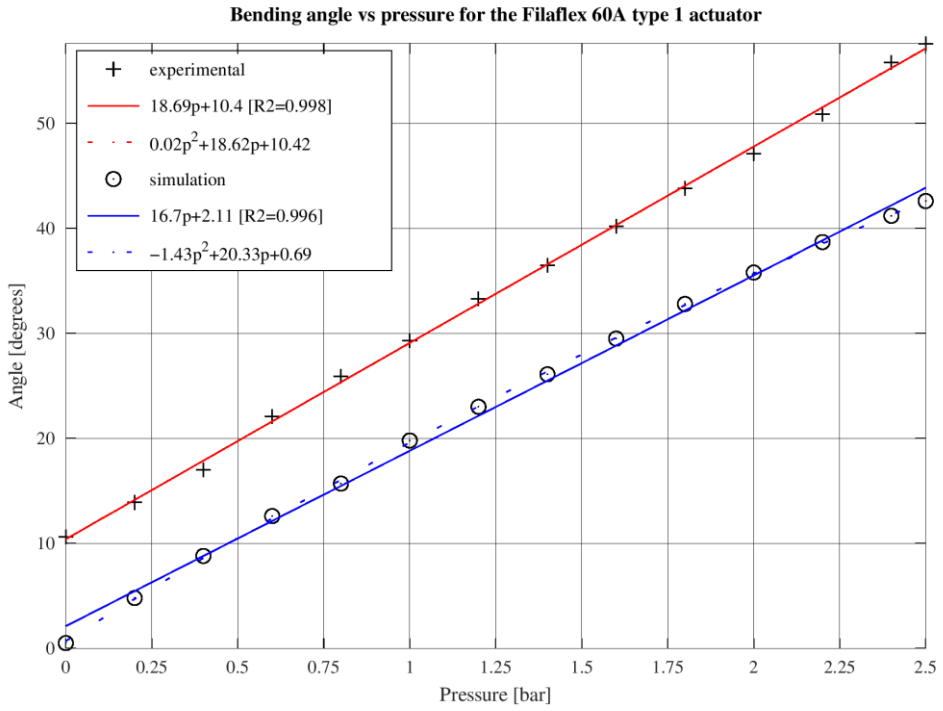

Figure 19. Bending angle vs. pressure for the Filaflex 60A type 1 actuator. Experimental data and simulation results.

It can be concluded that the use of FEM simulations is a very important tool to predict the natural behavior of the PneuNet actuators, enabling the designing and virtual testing of multiple configurations and the optimization of parameters such as lengths, thicknesses, materials, pressures, etc. to attain the best solutions.

In this study, considering the application of these actuators for the construction of a soft gripper for manipulation robotics, and although we have not carried out exhaustive tests to gauge longevity, nor made estimates of energy consumption or payload, nevertheless, some considerations can be made, and some comparisons can be made between them in terms of energy consumption, payload, and lifespan.

Energy consumption: Bearing in mind that the FilaFlex 60A and Elastosil M6401 A/B actuators require significantly higher pressures to achieve the curvatures required for gripping objects, this means that these actuators will consume more energy than the DragonSkin Fast 10 actuators. In addition, the on/off controller may be more energy efficient than the PI controller because the on/off controller generally results in the pump stopping for a large part of the gripper's closing action.

Payload: No payload tests have been carried out for each type of actuator or soft gripper, but it can be inferred that actuators made from stiffer materials, such as FilaFlex 60A and Elastosil M6401 A/B (in that order of stiffness), will be able to withstand a greater payload than actuators made from softer materials, such as DragonSkin Fast 10. In addition, the geometry of the actuator will also play a role in the payload, with actuators with larger and thicker geometry being able to withstand greater loads.

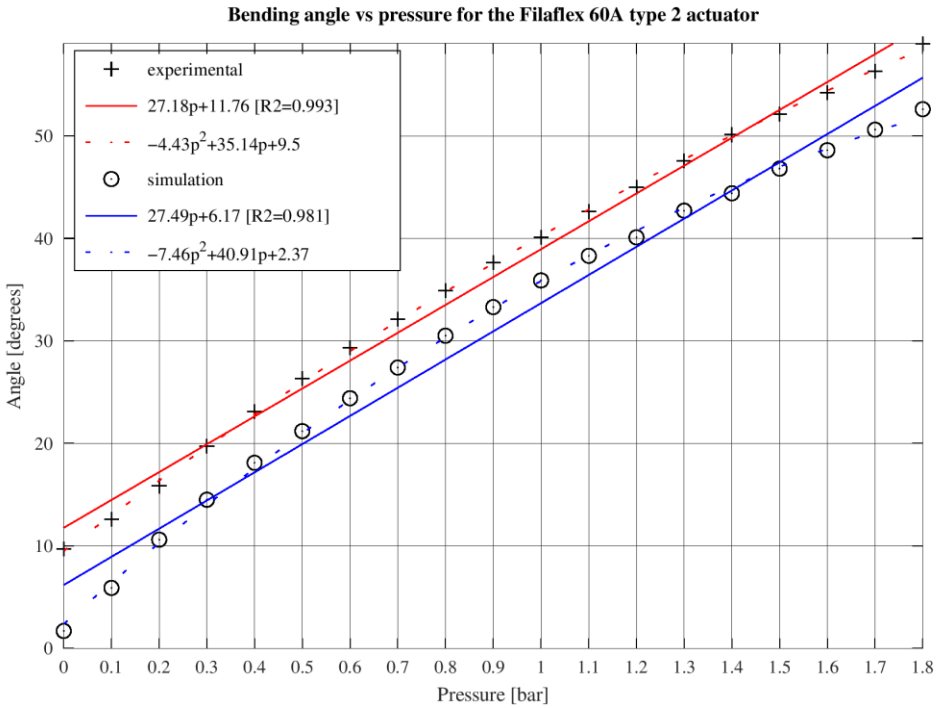

Figure 20. Bending angle vs. pressure for the Filaflex 60A type 2 actuator. Experimental data and simulation results.

Lifespan: Investigating the long-term durability of soft actuators under repeated use in the future will be crucial for practical applications. Although this study does not provide a specific estimate of the lifespan of the different actuators, it can be inferred that actuators made from more elastic materials, such as silicones, would have a longer lifespan than actuators made from less elastic, 3D-printed materials. But everything will depend on the frequency of use, the pressure levels used, and possible manufacturing defects, whether in the mold approach or by 3D printing. Actuators used more frequently and at higher pressures will probably fail sooner.

3.3.3. Data Analysis, Experimental Challenges, and Material Properties

Regarding the estimation of error in the experimental data, it is worth noting the difficulty of this estimation. We face two main challenges in determining this error. The first is associated with the calibration of the digital sensor, which was calibrated using an analog sensor with half the scale (0.25 bar). The second challenge lies in the parallax errors in the experimental setup for collecting angular values of the actuator using the Kinovea software. Although all care was taken in the setup and positioning of the camera and actuator, these measurements depend on the accuracy and repeatability of the experimental procedure, in addition to the computational and computer vision errors of the software for extracting data from the video. This is clearly a valid point for improvement in later study.

Experimental data exhibit an offset in the angular variable when compared to simulation results. For the Filaflex 60A material, experimental data are lower than finite element simulations; the opposite occurs for more flexible materials like DragonSkin and Elastosil. A possible explanation is the shape and magnitude of the force applied by the actuator's grip on the experimental support, and how this fixed constraint is imposed in the finite element simulation. However, more can be said by analyzing the angle's dependence on pressure.

The apparent linearity of the experimental angle data as a function of pressure, when a quadratic mathematical dependence would be expected, can be attributed to manufacturing processes. In the case of Filaflex 60A-printed actuators, the layered printing process introduces local anisotropies and alterations in the actuator's elastic parameters, which

could compensate for the effects of the actuator's constraint [16,18]. Additionally, the constant of the linear term depends on the elastic modulus, which is assumed to be constant. The hypothesis of a constant elastic modulus is not only a simplified approximation for hyperelastic materials but also drastically for metamaterials or composite materials, categories to which 3D-printed models naturally belong.

In the case of silicone actuators, manufacturing processes introduce anisotropies that are not accounted for in the underlying mathematical model. The fact that the actuator is constructed in two halves can introduce flexions and internal deformations in the material. Although care was taken to prevent the introduction of bubbles, their anisotropic distribution in the material undoubtedly introduces spatial variations in the elastic constants, breaking the uniformity and isotropy required by the mathematical model.

Another factor disrupting the mathematical model is the interaction of the gravitational force during actuator inflation. An anisotropic expansion of the material causes imbalances in internal forces, leading to preferential deformations in certain directions. These deformations, due to localized mass, are sources of deformations caused by gravity.

Although the causes of the nonlinear behavior are multiple and some of their effects are clearly visible in the analysis and results obtained, they do not invalidate the linear approximation, which well describes the universal behavior of this type of actuator as shown.

3.4. Control Results

This section presents results of pressure control experiments that were carried out to validate the proposed controllers. The gripper with soft actuators made of DragonSkin Fast 10® silicon was chosen for these experiments. Besides the results presented here, a series of experiments were performed to empirically adjust several control parameters to improve performance, namely, Kp, Ki, PWM_{ON}, threshold, and the throttle valve opening ratio. Although the influence of some of these parameters is interdependent (e.g., Kp and Ki), it has proved easy to find acceptable values for them through trial and error. This procedure led to the following constants, which were used in the experiments reported below.

Kp = 5000 bar^{-1};
Ki = 2000 bar^{-1} s^{-1};
Dt = 10 ms;
Threshold = 0.01 bar;
Throttle valve opening ratio = 5%.

Additionally, readings from the pressure sensor (model NBPDANN150PAUNV [29]) were filtered through a low pass filter with a cutoff frequency of 6.8 Hz.

All experiments consist of system step responses, with the desired pressure being varied from zero to a positive pressure and back to zero. This waveform of the desired pressure results in consecutively closing and opening the gripper. To test closing the gripper with different soft actuator angles, step responses were obtained for goal pressures in the set {0.1, 0.15, 0.2, 0.25} bar.

Nonlinear PI controller

Figure 21a shows the results obtained with the nonlinear PI controller, depicting the pressure and the control actions for the different input levels. This figure makes it clear that there are qualitative differences in the responses with the variation in the input level, which is a manifestation of the nonlinearities of the system and demonstrates the need to consider the range of the desired pressure when designing the controller. Most notably, the oscillatory behavior becomes less pronounced as the reference pressure increases and disappears entirely at 0.25 bar.

In two underdamped cases, the overshoot causes the controller to open the valve, which results in a pressure drop that is later compensated by the pump action. The throttle valve opening ratio has been adjusted so that this pressure drop is smooth enough not to cause further oscillations. This results in a longer time for the gripped opening, represented

in this figure by the responses to the falling step in the reference. At the higher reference pressure (0.25 bar), the transition to the ambient pressure takes about 0.8 s.

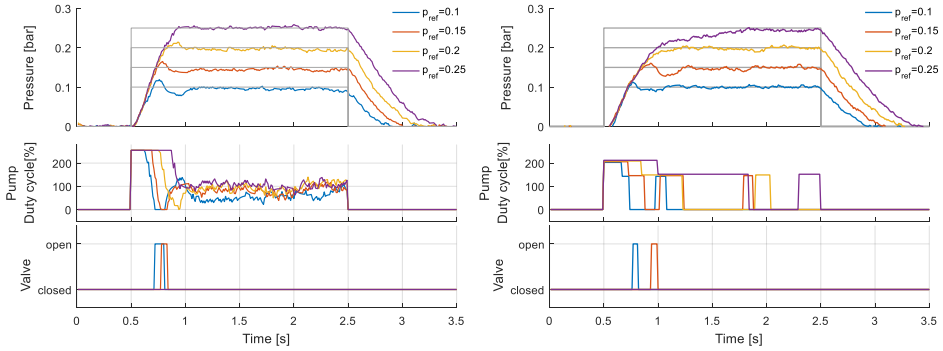

(a) (b)

Figure 21. Results with a PI controller (**a**) and with an on/off controller (**b**).

On/Off controller

The results obtained with the on/off controller (Figure 21b) show some similarities with those of the PI controller regarding oscillatory behavior. Notably, it used two values of the duty cycle for the on state of the pump: a higher value, 80%, if the error is larger than 5× threshold, and a lower value, 60%, for lower errors. In this way, it was possible to obtain a fast response at the beginning of the step input, due to the higher duty cycle, and at the same time avoid large overshoots, by using a lower duty cycle at lower error values. A comparison of the control actions of the two controllers reveals an advantage of the on/off controller: in most cases, this controller results in the pump being switched off for a large part of the gripper closing action. With the PI controller, on the other hand, the control action assumes significant values for the entire duration of the same period. This is due to the accumulation of errors and the fact that the pump motor stalls at higher pressures and therefore does not contribute to eliminating the error. This not only leads to a waste of energy but also to a deterioration in the performance of the motor.

Response Time

Soft grippers are known to react more slowly than their rigid counterparts, which can move very quickly, especially when they are pneumatically driven. In our experiments, the fastest closing times were achieved with the PI controller, where the 5% margin around the desired pressure was always achieved within an interval of 0.6 s. The on/off controller generally led to longer response times, which is due to the fact that the control action does not depend on the error but is fixed in advance. The opening time does not depend on the controller but on the reference pressure and the degree of opening of the throttle valve. Assuming that the release of the load is achieved when pressure has dropped to 50% of the reference pressure, it can be seen that this is achieved within 0.35 s in all our tests.

4. Conclusions

This study presents the design, control, and testing of a multifunctional soft robotic gripper for a Dobot robot based on pneumatic network (PneuNet) bending actuators. Two different models of PneuNet actuators were successfully developed using three materials: FilaFlex 60A (3D-printed), Elastosil M4601, and Dragonskin Fast 10 silicones (molded). The research demonstrates the viability of both 3D printing and molding techniques for fabricating soft robotic actuators, with each method offering unique advantages in terms of material properties and manufacturing processes.

Finite Element Method (FEM) simulations proved to be a valuable tool in predicting the behavior of PneuNet actuators. The simulations, using hyperelastic material models (Yeoh for silicones and Mooney–Rivlin for FilaFlex 60A), showed good correlation with experimental results for the silicone-based actuators. However, significant discrepancies

were observed in the FDM-printed FilaFlex 60A actuators, where the predicted bending angle was consistently much lower than the experimentally measured angle. This suggests that the hyperelastic FEM models using the second-order Mooney–Rivlin model may be overly stiff for these 3D-printed materials, highlighting the need for further refinement of simulation parameters to accurately represent the behavior of 3D-printed soft actuators.

A key finding of this study is that the type 2 actuator, inspired by Patel et al. [19], demonstrates a greater bending angle than the type 1 actuator, inspired by Yap et al., for the same applied pressure. This result has important implications for design optimization in soft robotic applications. Additionally, it was observed that FDM Elastosil actuators require significantly higher pressures to achieve the necessary curvatures for object grasping. While this higher-pressure requirement increases the operational costs due to compressor usage and elevates the risk of sudden rupture, the FDM printing method offers unparalleled freedom and speed in prototyping and producing new designs. This trade-off between performance, cost, and manufacturing flexibility presents an important consideration for future soft robotic gripper designs.

The results of this study lead to a crucial conclusion regarding material properties: actuators with a greater elastic component (lower Young's Modulus) yield more flexible results, achieving a greater range of movement with lower input pressures. This finding underscores the importance of material selection in soft robotic design, particularly when the goal is to maximize flexibility and minimize operational pressures. It suggests that softer, more elastic materials may be preferable for applications requiring large deformations at low pressures, while stiffer materials might be better suited for applications requiring higher force output or precision.

The implementation of both nonlinear PI and on/off controllers for the pneumatic system demonstrated effective pressure control in the soft actuators. The controllers were able to manage the inherent nonlinearities and delays in the pneumatic system, with the on/off controller showing potential energy efficiency advantages. The addition of a throttle valve proved crucial in mitigating oscillatory behavior, especially at lower pressures. These control strategies offer a balance between performance and simplicity, making them suitable for practical applications of soft robotic grippers.

Future research should focus on refining the FEM models, particularly for 3D-printed materials, to better predict their behavior under various operating conditions. Exploration of advanced control algorithms to further improve performance and energy efficiency is also warranted. Additionally, investigating the long-term durability of the soft actuators under repeated use, especially for the higher-pressure FDM actuators, will be crucial for practical applications. The integration of embedded sensors for closed-loop control and the exploration of more complex gripper designs could enhance the versatility and precision of the soft robotic system. Further research into the relationship between material properties, particularly elasticity, and actuator performance could lead to the development of new materials specifically tailored for soft robotic applications. This research contributes to the growing field of soft robotics, offering insights into the design, fabrication, and control of compliant grippers for sensitive object manipulation, while highlighting the complex trade-offs between manufacturing methods, material properties, and actuator performance.

Author Contributions: Conceptualization, A.C., T.C., F.C., and M.J.G.C.M.; methodology, A.C., T.C., F.C., and M.J.G.C.M.; software, A.C., A.L., and F.C.; validation, A.C., T.C., A.L., F.C., and M.J.G.C.M.; investigation, A.C., T.C., F.C., A.R., and M.J.G.C.M.; resources, T.C., F.C., N.M., A.R., and M.J.G.C.M.; writing—original draft preparation, A.C., T.C., A.L., F.C., and M.J.G.C.M.; writing—review and editing, F.C., N.M., A.R., and M.J.G.C.M.; supervision, T.C., and M.J.G.C.M.; project administration, M.J.G.C.M.; funding acquisition, M.J.G.C.M. All authors have read and agreed to the published version of the manuscript.

Funding: This research was funded by Instituto Politécnico de Lisboa by the project number: IPL/IDI&CA2023/ACTSOFTLY_ISEL.

Data Availability Statement: The original contributions presented in this study are included in the article, and further inquiries can be directed to the corresponding author.

Conflicts of Interest: The authors declare no conflicts of interest.

References

1. Robotics, D. Magician Robot—Desktop Grade Robot for Advanced Education. Available online: https://www.dobot-robots.com/products/education/magician.html (accessed on 28 September 2024).
2. Rus, D.; Tolley, M.T. Design, Fabrication and Control of Soft Robots. *Nature* **2015**, *521*, 467–475. [CrossRef] [PubMed]
3. Tawk, C.; Alici, G. A Review of 3D-Printable Soft Pneumatic Actuators and Sensors: Research Challenges and Opportunities. *Adv. Intell. Syst.* **2021**, *3*, 2000223. [CrossRef]
4. El-Atab, N.; Mishra, R.B.; Al-Modaf, F.; Joharji, L.; Alsharif, A.A.; Alamoudi, H.; Diaz, M.; Qaiser, N.; Hussain, M.M. Soft Actuators for Soft Robotic Applications: A Review. *Adv. Intell. Syst.* **2020**, *2*, 2000128. [CrossRef]
5. Pratt, G.A.; Williamson, M.M. Series Elastic Actuators. *IEEE Int. Conf. Intell. Robot. Syst.* **1995**, *1*, 399–406. [CrossRef]
6. Ham, R.; Sugar, T.; Vanderborght, B.; Hollander, K.; Lefeber, D. Compliant Actuator Designs. *IEEE Robot. Autom. Mag.* **2009**, *16*, 81–94. [CrossRef]
7. Mosadegh, B.; Polygerinos, P.; Keplinger, C.; Wennstedt, S.; Shepherd, R.F.; Gupta, U.; Shim, J.; Bertoldi, K.; Walsh, C.J.; Whitesides, G.M. Pneumatic Networks for Soft Robotics That Actuate Rapidly. *Adv. Funct. Mater.* **2014**, *24*, 2163–2170. [CrossRef]
8. Ang, B.W.K.; Yeow, C.H. 3D Printed Soft Pneumatic Actuators with Intent Sensing for Hand Rehabilitative Exoskeletons. In Proceedings of the 2019 International Conference on Robotics and Automation, Montreal, QC, Canada, 20–24 May 2019; pp. 841–846. [CrossRef]
9. Kim, S.; Laschi, C.; Trimmer, B. Soft Robotics: A Bioinspired Evolution in Robotics. *Trends Biotechnol.* **2013**, *31*, 287–294. [CrossRef]
10. Shepherd, R.F.; Ilievski, F.; Choi, W.; Morin, S.A.; Stokes, A.A.; Mazzeo, A.D.; Chen, X.; Wang, M.; Whitesides, G.M. Multigait Soft Robot. *Proc. Natl. Acad. Sci. USA* **2011**, *108*, 20400–20403. [CrossRef]
11. Ogura, K.; Wakimoto, S.; Suzumori, K.; Nishioka, Y. Micro Pneumatic Curling Actuator -Nematode Actuator-. In Proceedings of the 2008 IEEE International Conference on Robotics and Biomimetics, Bangkok, Thailand, 22–25 February 2009; pp. 462–467. [CrossRef]
12. Gu, G.; Wang, D.; Ge, L.; Zhu, X. Analytical Modeling and Design of Generalized Pneu-Net Soft Actuators with Three-Dimensional Deformations. *Soft Robot.* **2021**, *8*, 462–477. [CrossRef]
13. Wilson, J.F. Mechanics of Bellows: A Critical Survey. *Int. J. Mech. Sci.* **1984**, *26*, 593–605. [CrossRef]
14. Sudani, M.; Deng, M.; Wakimoto, S. Modelling and Operator-Based Nonlinear Control for a Miniature Pneumatic Bending Rubber Actuator Considering Bellows. *Actuators* **2018**, *7*, 26. [CrossRef]
15. Peng, Y.; Nabae, H.; Funabora, Y.; Suzumori, K. Controlling a Peristaltic Robot Inspired by Inchworms. *Biomim. Intell. Robot.* **2024**, *4*, 100146. [CrossRef]
16. Rad, C.; Hancu, O.; Lapusan, C. Data-Driven Kinematic Model of PneuNets Bending Actuators for Soft Grasping Tasks. *Actuators* **2022**, *11*, 58. [CrossRef]
17. Majidi, C.; Shepherd, R.F.; Kramer, R.K.; Whitesides, G.M.; Wood, R.J. Influence of Surface Traction on Soft Robot Undulation. *Int. J. Robot. Res.* **2013**, *32*, 1577–1584. [CrossRef]
18. Alici, G.; Canty, T.; Mutlu, R.; Hu, W.; Sencadas, V. Modeling and Experimental Evaluation of Bending Behavior of Soft Pneumatic Actuators Made of Discrete Actuation Chambers. *Soft Robot.* **2018**, *5*, 24–35. [CrossRef]
19. Yap, H.K.; Ng, H.Y.; Yeow, C.-H. High-Force Soft Printable Pneumatics for Soft Robotic Applications. *Soft Robot.* **2016**, *3*, 144–158. [CrossRef]
20. Patel, D.K.; Sakhaei, A.H.; Layani, M.; Zhang, B.; Ge, Q.; Magdassi, S. Highly Stretchable and UV Curable Elastomers for Digital Light Processing Based 3D Printing. *Adv. Mater.* **2017**, *29*, 1606000. [CrossRef]
21. Smooth-On Dragon Skin™ 10 FAST. Available online: https://www.smooth-on.com/products/dragon-skin-10-fast/ (accessed on 29 September 2024).
22. Wacker Chemie AG. ELASTOSIL® M 4601 A/B. Room Temperature Curing Silicone Rubber (RTV-2). Available online: https://www.wacker.com/h/en-us/medias/ELASTOSIL-M-4601-AB-en-2024.06.16.pdf (accessed on 29 September 2024).
23. Recreus Filaflex 60A. Available online: https://recreus.com/gb/filaments/1-1-filaflex-60a.html#/1-colour-black/2-diameter-175_mm/3-weight-500_gr (accessed on 29 September 2024).
24. Oh, H.-A.; Park, D.; Han, K.-S.; Oh, T.S. Elastic Modulus of Locally Stiffness-Variant Polydimethylsiloxane Substrates for Stretchable Electronic Packaging Applications. *J. Microelectron. Packag. Soc.* **2015**, *22*, 91–98. [CrossRef]
25. Adafruit Industries Air Pump and Vacuum DC Motor—4.5 V and 2.5 LPM [ZR370-02PM]: ID 4699: Adafruit Industries, Unique & Fun DIY Electronics and Kits. Available online: https://www.adafruit.com/product/4699 (accessed on 7 November 2024).
26. Adadruit Industries 6V Air Valve with 2-Pin JST XH Connector [FA0520E]: ID 4663: Adafruit Industries, Unique & Fun DIY Electronics and Kits. Available online: https://www.adafruit.com/product/4663 (accessed on 7 November 2024).
27. Hi-Tech Flow Control Valve 4mm M5 | E-Pneumatic Store. Available online: https://www.e-pneumatic.com/valves/manual-throttle-valves/flow-valve-04-m5.html (accessed on 20 November 2024).
28. Honeywell. *Basic Board Mount Pressure Sensors*; Datasheet 32307741; Honeywell: Charlotte, NC, USA, 2024.

29. Gerboni, G.; Diodato, A.; Ciuti, G.; Cianchetti, M.; Menciassi, A. Feedback Control of Soft Robot Actuators via Commercial Flex Bend Sensors. *IEEE/ASME Trans. Mechatron.* **2017**, *22*, 1881–1888. [CrossRef]
30. Wang, T.; Zhang, Y.; Chen, Z.; Zhu, S. Parameter Identification and Model-Based Nonlinear Robust Control of Fluidic Soft Bending Actuators. *IEEE/ASME Trans. Mechatron.* **2019**, *24*, 1346–1355. [CrossRef]
31. Chen, C.; Tang, W.; Hu, Y.; Lin, Y.; Zou, J. Fiber-Reinforced Soft Bending Actuator Control Utilizing On/Off Valves. *IEEE Robot. Autom. Lett.* **2020**, *5*, 6732–6739. [CrossRef]
32. Memarian, M.; Gorbet, R.; Kulic, D. Control of Soft Pneumatic Finger-like Actuators for Affective Motion Generation. In Proceedings of the IEEE International Conference on Intelligent Robots and Systems, Hamburg, Germany, 28 September–2 October 2015; Institute of Electrical and Electronics Engineers Inc.: Piscataway, NJ, USA, 2015; pp. 1691–1697.
33. Elgeneidy, K.; Lohse, N.; Jackson, M. Bending Angle Prediction and Control of Soft Pneumatic Actuators with Embedded Flex Sensors—A Data-Driven Approach. *Mechatronics* **2018**, *50*, 234–247. [CrossRef]
34. Ibrahim, S.; Krause, J.C.; Raatz, A. Linear and Nonlinear Low Level Control of a Soft Pneumatic Actuator. In Proceedings of the RoboSoft 2019 2nd IEEE International Conference on Soft Robotics, Seoul, Republic of Korea, 14–18 April 2019; Institute of Electrical and Electronics Engineers Inc.: Piscataway, NJ, USA, 2019; pp. 434–440.
35. Luo, M.; Skorina, E.H.; Tao, W.; Chen, F.; Ozel, S.; Sun, Y.; Onal, C.D. Toward Modular Soft Robotics: Proprioceptive Curvature Sensing and Sliding-Mode Control of Soft Bidirectional Bending Modules. *Soft Robot.* **2017**, *4*, 117–125. [CrossRef] [PubMed]
36. Skorina, E.H.; Luo, M.; Ozel, S.; Chen, F.; Tao, W.; Onal, C.D. Feedforward Augmented Sliding Mode Motion Control of Antagonistic Soft Pneumatic Actuators. In Proceedings of the 2015 IEEE International Conference on Robotics and Automation, Seattle, WA, USA, 26–30 May 2015; Institute of Electrical and Electronics Engineers Inc.: Piscataway, NJ, USA, 2015; pp. 2544–2549.
37. Skorina, E.H.; Luo, M.; Tao, W.; Chen, F.; Fu, J.; Onal, C.D. Adapting to Flexibility: Model Reference Adaptive Control of Soft Bending Actuators. *IEEE Robot. Autom. Lett.* **2017**, *2*, 964–970. [CrossRef]
38. Arena, P.; Famoso, C.; Noce, A.L.; Motta, A.; Galati, I.; Patanè, L. A New Motor-Neuron Circuit Implementation. In Proceedings of the 2024 IEEE International Symposium on Circuits and Systems, Singapore, 19–22 May 2024; Institute of Electrical and Electronics Engineers Inc.: Piscataway, NJ, USA, 2024.
39. Ogata, K. *Modern Control Engineering*, 5th ed.; Pearson: London, UK, 2009; ISBN 13: 9780136156734.
40. Muddada, R. Design, Modeling, and Comparative Analysis on Silicone Rubber Soft Gripper for Food Industry. *Int. Res. J. Mod. Eng. Technol. Sci.* **2021**, *3*, 2582–5208.
41. ANSYS ANSYS Mechanical: Advanced Nonlinear Materials—Appendix 4A: Hyperelasticity. Available online: https://innovationspace.ansys.com/courses/wp-content/uploads/sites/5/2024/01/8_Modulus-vs-Strain-data.pdf (accessed on 19 November 2024).
42. Dezaki, M.L.; Bodaghi, M.; Serjouei, A.; Afazov, S.; Zolfagharian, A. Soft Pneumatic Actuators with Controllable Stiffness by Bio-Inspired Lattice Chambers and Fused Deposition Modeling 3D Printing. *Adv. Eng. Mater.* **2023**, *25*. [CrossRef]